BOREHOLE EFFECT CAUSING ARTEFACTS IN CROSS-BOREHOLE ELECTRICAL RESISTIVITY TOMOGRAPHY: A HYDRAULIC FRACTURING CASE STUDY

M.T. Perri[1], I. Barone[1], G. Cassiani[1,], R. Deiana[2], A. Binley[3]*

[1] Dipartimento di Geoscienze, Università di Padova, Padova, via Gradenigo 6, 35131, Italy

[2] Dipartimento di Beni Culturali, Università di Padova, Padova, piazza Capitaniato 7, 35139, 35131, Italy

[3] Lancaster Environment Centre, Lancaster University, Lancaster, LA1 4YQ, United Kingdom

[*]Corresponding author. *E-mail address:* giorgio.cassiani@unipd.it.

Address: Dipartimento di Geoscienze, Università di Padova, Padova, via Gradenigo 6, 35131, Italy. *Tel:* +39 049 8279189.

Authors' e- mail addresses: mariateresa.perri@unipd.it (M.T. Perri), ilaria.barone@phd.unipd.it (I. Barone); giorgio.cassiani@unipd.it (G. Cassiani), rita.deiana@unipd.it (R. Deiana), a.binley@lancaster.ac.uk (A. Binley)

Submitted for publication to the *Near Surface Geophysics Special Issue on Geoelectrical Monitoring: advances in measurement and modelling for environmental and engineering applications.*

May 18, 2020

ABSTRACT

Electrical resistivity tomography (ERT) is a technique widely used for the investigation of the structure and fluid-dynamics of the shallow subsurface, particularly for hydro-geophysical purposes, sometimes using cross-borehole configurations. The results of ERT inversion and their usefulness in solving hydrogeophysical problems, even though invariably limited by resolution issues, depend strongly on the accuracy of inversion, which in turns depends on a proper estimation and handling of data and model errors. Among model errors, one approximation often applied in cross-hole ERT is that of neglecting the effects of boreholes and the fluids therein. Such effects inevitably impact the current and potential patterns as measured by electrodes in the boreholes themselves. In presence of very saline fluids, in particular, this model approximation may prove inadequate and the tomographic inversion may yield images strongly contaminated by artefacts. In this paper we present a case study where highly saline water was used for hydraulic fracturing to improve permeability of a shallow formation impacted by hydrocarbon contamination, with the final aim of improving the effectiveness of in situ contaminant oxidation. The hydraulic fracturing was monitored via time-lapse cross-hole ERT. Arrival of the saline water in the monitoring borehole likely caused a strong borehole effect that significantly affected the quality and usefulness of ERT inversions. In this paper we analyse the experimental dataset and produce, via 3D ERT forward modelling, a viable explanation for the observed, paradoxical field results.

Keywords: ERT, electrical resistivity tomography, cross-hole methods, borehole effect, tracer test.

1. INTRODUCTION

During the last three decades electrical resistivity tomography (ERT), in particular in cross-hole mode, has been shown to be useful for several environmental and engineering applications, including, among others, site characterization, groundwater process monitoring, LNAPLs and DNAPLs detection (*e.g.* LaBrecque et al., 1996a; Slater et al., 2000; Binley et al., 2002, Cassiani et al., 2006; Deiana et al., 2007; Wagner et al., 2015). ERT has long progressed beyond the traditional mapping of geophysical “anomalies”, in order to provide time-lapse 2D/3D data that can be used, for example, as input to flow and transport models or as informative tools to vulnerability and environmental assessment procedures. As geotechnical, environmental and remediation projects often require detailed information at depth, cross borehole ERT is preferable to surface resistivity imaging due to its better vertical resolution capability.

In cross borehole ERT the electrodes are installed into two or more boreholes, placed in contact with the host soils/rocks or with the formation fluid, thus providing highly informative data at depth. Depending on the geological setting and logistical aspects in the study area, there are different ways of installing these electrodes into the subsurface and obtaining the electrical contact between them and the surrounding media. In dry holes, for example, mud, sand or concrete grout may be used to backfill the boreholes and completely cover the electrodes. At sites where groundwater is close to the surface, the electrodes can be installed putting a water-tight electrical cable down the measurement boreholes, simply verifying that the string of electrodes lies entirely below the water table.

Although the presence of a conductive medium inside or around the boreholes is hence necessary to guarantee the electrical contact at depth, this medium could be considered at the same time a source of disturbance to the experimental data, as such a medium does not possess the same electrical properties as the geological medium under investigation. Some negative impacts on the collection and inversion of cross-borehole ERT data can in fact be potentially related to the well known *borehole effect* in wire-line electrical logging literature (Keller and Frischknecht, 1966; Keys and MacCary, 1971; Telford et al., 1990). This effect derives from the contrast existing between the resistivity of the soil/rock formation (ρ_r) and that of the borehole backfill material or fluid (ρ_f) and usually results in a narrow cylindrical anomaly; the value of ρ_r is commonly higher than ρ_f, thus the current will tend to flow along the borehole axis limiting radially outward flow into the formation. Such a resistivity contrast, especially when it reaches large values, inevitably impacts the current and potential patterns as measured by electrodes in the boreholes.

In most cases, however, the ρ_r / ρ_f value is often assumed a priori to be small and hence not considered in forward and inverse models. This is understandable in cases where the formation fluid fills the borehole, and thus the ρ_r / ρ_f ratio equals the formation factor *F*, and also when the porosity is relatively large as in clastic formations, thus keeping *F* within relatively small values (< 10). A few researchers have focused their attention on the borehole effect issue (Daily and Ramirez, 1995; Osiensky et al., 2004; Daily et al., 2005; Nimmer et al., 2008; Doetsch et al., 2010; Wagner et al., 2015), demonstrating that, particularly in presence of very saline fluids, neglecting the effect of boreholes and the fluid therein may prove inadequate and can give rise to inversion artefacts. Osiensky et al. (2004) and Nimmer et al. (2008), in particular, demonstrated that apparent resistivity values in cross-borehole ERT experiments are significantly influenced by the borehole fluids. Unless the effects of the borehole fluids are accounted for, either by explicitly including the boreholes in the modelling mesh/grid or possibly by applying correction factors to the raw data (see *e.g.* Doetsch et al., 2010), common regularized tomographic inversions are likely to yield images contaminated with artefacts. Some of the artefacts in

ERT images will be obvious, *e.g.*, anomalous features along the lengths of the boreholes, and thus may not affect the usefulness of the ERT image. Other artefacts might not be that easy to identify.

The need for an accurate data quality assessment and modelling is hence necessary, especially when dealing with a methodology that is limited by further resolution issues (*e.g.* Day-Lewis et al., 2005) and when the main target of the study is an estimation of subsurface parameters. This is, for example, the case in the application of electrical resistivity techniques to monitoring saline tracer tests for hydrogeological or environmental purposes. Geophysical time-lapse models may be interpreted in terms of transport parameters, as demonstrate by previous studies of time-lapse ERT applied to tracer tests (*e.g.* Kemna et al., 2002; Daily et al., 2004, Kemna et al., 2006; Camporese et al., 2011, 2015; Perri et al., 2012; Coscia et al., 2012; Crestani et al., 2015; Lekmine et al., 2017; Busato et al., 2019). However, the interpretation of solute tracer experiments is made difficult by the uncertainty related to the data modeling and inversion and a rigorous approach is hence mandatory to reduce such uncertainty.

In this paper, we present an example of ERT applied to a saline tracer test. In particular, we analyse the results of a series of time-lapse 2D ERT surveys that were carried out at a contaminated site near Trento, north east Italy. The purpose of the surveys was to monitor the effectiveness of hydraulic fracturing (indeed in loose sediments this may result more precisely in fissuring, but “hydraulic fracturing” is the technical term) performed on a hydrocarbon-contaminated silt formation, in order to increase its hydraulic conductivity and enhance the effectiveness of the proposed in-situ remediation technique (ozone oxidation). The fluid used for hydraulic fracturing was a nearly-saturated NaCl brine, the arrival of which in nearby boreholes is traditionally monitored via down-hole electrical conductivity meters. Cross-borehole ERT was proposed and implemented as an additional imaging technique to assess the effectiveness of brine migration following fracturing, since ERT is sensitive to conductivity contrasts at depth.

The goal of this paper is to highlight both the powerful application of such an integrated monitoring methodology and the possible drawbacks. Special attention will be paid, in particular, to the limitation deriving from *borehole effect* to data collection and inversion, thus advocating great caution in making reliable interpretation of field measurements.

2. CASE STUDY

The experimental site of interest is located in the northern part of the city of Trento, in the Trentino Alto–Adige Region (north east Italy), along the left bank of the Adige River (Figure 1). The area, also known as the “Trento-Nord” site, was an important industrialized suburb: since the early 1900s the site housed large industrial operations, mainly carried out by two chemical companies. In the last decade of the twentieth century, due to severe contamination episodes linked to uncontrolled industrial emissions, the “Trento – Nord” site was added to the Italian National Priority List of contaminated sites and is currently waiting for final site assessment and remediation.

Environmental assessment activities, particularly in the area considered in this study, revealed the presence of high levels of organic contaminants in the subsurface and forced the chemical industry to stop its production activity. The main product of this industry was phthalic anhydride, an organic compound derived from ortho-xylene, naphthalene and their mixtures. Among others techniques, in-situ ozonation was selected as the most efficient method to remediate soil and groundwater pollution, due to the ozone high capability to oxidise organic contaminants to safe levels. Furthermore, this is an ‘environmentally friendly’ treatment since ozone is produced on-site from oxygen and reverts back to oxygen after reacting with contaminants.

In a very permeable matrix, in-situ ozone hydrocarbon oxidation appears to be very successful. In presence of relatively low permeability soils, as is the case of the present study (see later), the treatment may, however, be long and costly. For this reason hydraulic fracturing has been tested in conjunction with ozonation. By hydraulic fracturing, pressurized water is injected through wells to develop cracks in low permeability sediments. The enhanced permeability increases the effectiveness of in-situ processes and enhances extraction efficiency by increasing contact areas between contaminants adsorbed onto soil particles and the extraction medium.

In order to evaluate the actual volume of influence of the procedure and prevent potential mitigation measures linked to uncontrolled fracture propagation, a preliminary phase of hydraulic fracturing testing must be performed to assess the best water injection rate and pressure values. If these values are too low, the resulting weak water diffusion would lead to an insufficient remediation treatment; in contrast, excessively high values would result in the creation of few, wide fractures, thus limiting the effectiveness of the remediation. Furthermore, the fractures created should ideally extend laterally within the zone of interest; however, substantial vertical fracture propagation may also occur, significantly impacting the success of the treatment.

In the case considered, time-lapse ERT was used to help define the effectiveness of the hydraulic fracturing test and consequently increase the probabilities of success of remediation procedure. The saline nature of the tracers generally used to be detected via down-hole electrical conductivity meters (*e.g.* NaCl, KCl and KBr aqueous solutions) can be easily mapped by ERT, due to the sharp electrical conductivity contrast with fresh natural groundwater. Furthermore, time-lapse ERT may retrieve complete 2D/3D time-lapse images of the tracer migration, thus having a clear advantage over traditional localized borehole sampling methods. However, some difficult aspects related to data interpretation, in particular those deriving from borehole effects and to the presence of a highly conductive pore fluid, will be discussed in order to gain some general insight into the quality of information that can or cannot be retrieved by such an application.

3. GEOLOGICAL AND HYDROGEOLOGICAL SETTING

The territory is located in the alluvial plain of Adige River near the city of Trento, delimited laterally by the massive carbonate formations of the Soprassasso and Calisio Mountains, and partially covered by the alluvial fan deposits of the Avisio and Fersina Streams, two left tributaries of the Adige river.

Geological investigations carried out on site by the geological department of the local authorities ("Provincia Autonoma di Trento") identified the presence of a sequence of unconsolidated sediments deposited by the Adige during the Quaternary age, in particular between the end of the Upper Pleistocene stage and the present age. The grain size distribution of these postglacial fluvial deposits ranges from fine to medium-fine and medium-large sediments. In particular, the local soil type ranges from clayey silt and sandy silt to silty sand and sand with gravel, in a mainly alkaline soil. These alluvial deposits can reach a depth of several tens of meters and are characterized by inclination angles that do not exceed a few degrees (ISPRA Ambiente- Note Illustrative al Foglio n. 60 "Trento").
At the scale of study and on the basis of several available stratigraphic logs from previous environmental investigations, the soil profile of the "Trento – Nord" site from the ground surface to the maximum depth of interest (about 14 m) can be summarized as a layered

sequence of (Figure 2): a thin layer of debris from building demolition about 1 m thick, a silty soil layer between about 1 and 6 m, a layer of sand with gravel between about 6 and 14 m, and finally a bottom layer of clay and sandy silt with organic matter starting from 14 m.

From a hydrogeological perspective, the “Trento-Nord” site is characterized by the presence of a semi-confined aquifer (the sand/gravel layer), with an average hydraulic conductivity (K) value of about 3×10^{-3} m/s and a mean hydraulic gradient as measured from piezometric surveys equal to 0.1-0.2% towards the southeast. Depth to groundwater ranges between 2 and 4 m from the ground surface.

4. FIELD METHODOLOGY

The environmental assessment activities carried out on the “Trento-Nord” site revealed that the entire soil section in the depth range from 0 to about 8 m is heavily contaminated by organic compounds. In particular, soil samples collected at different depths from the silty formation overlying the horizon of sand with gravel (see Figure 2) showed the highest concentrations of naphthalene and phenols. Unfortunately, the aquifer is continuously recharged from precipitation and inflow of Adige river waters, and the contamination has migrated deeper into the saturated zone.

Pilot-scale experiments in an area approximately 12 m by 20 m (Figure 3) were designed and performed, with the aim of evaluating the above-mentioned in-situ remediation procedure parameters, prevent leak-off of treatment fluids into the high permeability horizons overlying and underlying the contaminated silty formation, and evaluate the extent of the aquifer that is potentially remediable.

For these purposes, the pilot-scale tests have been monitored by an integrated approach, using both traditional tracer test methods (in-hole electrical conductivity meters) in conjunction with time-lapse cross-borehole ERT techniques. The test procedure was as follows: (1) in the first phase, a volume of pure water was injected into subsurface (for details on boreholes layout, see later) at a flow rate and a pressure necessary to exceed the natural formation strength and create a network of fractures (the orientation of fractures depending on the in-situ stress field); (2) a volume of saline solution was subsequently injected into the formation (and fractures) at the same flow rate as above and used as tracer to be detected by down-hole conductivity meters; (3) in order to retrieve a complete 2D/3D time-lapse image of the tracer evolution and consequently evaluate the radius of fluid intrusion (i.e. the spatial extent of fractures), several time lapse 2D ERT surveys in cross-borehole mode were performed during the tracer tests.

The saline tracer used in the experiment was prepared on site by mixing NaCl into about 1 m^3 of drinking water, to achieve a resulting groundwater electrical conductivity of about 145 mS/cm (in contrast to the background, pre-injection, groundwater conductivity equal roughly to 1 mS/cm – *i.e.* a resistivity of 10 Ωm). Gravitational sinking effects of the nearly-saturated NaCl brine, which in general lead to negative occurrences in data collection (such as loss of signal), did not have any consequences in this case, due to the low permeability values of the medium of interest and the forced flow conditions that have been maintained during the saline tracer tests.

To inject and monitor the saline tracer in the subsurface, a dense network of boreholes (labelled *0* to *9* – see Figure 3) was drilled. The boreholes were completed with a 2” (50mm) fully slotted plastic casing to a depth of about 10 m, except the boreholes *0, 7, 8,* and *9* that reached a depth of about 14 m. The monitoring boreholes were placed along two perpendicular directions in order to retrieve, and consequently compare, two different responses to field tests. The cores were extracted and retained to be analyzed in laboratory to provide the site stratigraphy (see Figure 2). One of the deepest boreholes (*0*) was originally used as the tracer injection point, the boreholes *1* to *6* being designed to be used for ERT data collection and located at increasing distances (2, 4 and 6 m respectively, see Figure 3). During some preliminary testing procedures, however, borehole *0* became clogged, and boreholes *2* and *3* were therefore used as injection points. In order to perform the tracer injection in boreholes *2* and *3,* a specific depth section was isolated with inflatable double packers placed respectively at 7.5 and 8 m depth. The brine injection with hydraulic fracturing lasted about 1 hour (considering an injection rate of about 3 to 6 m^3/h and a pressure of about 0.8 bar), after which a large volume of non saline water was introduced in the injection system to wash out the brine and re-establish the pre-injection electrical conditions of the system. For the entire duration of the test (a few hours), the in situ water electrical conductivity was monitored by the down-hole electrical conductivity meters placed in each borehole.

Repeated ERT acquisitions in cross-hole mode were performed before and during the tracer tests. To achieve this, two water-tight electrical cables, each equipped with 24 electrodes, spaced 0.4 m, were introduced in the monitoring boreholes *1* - *4* (when using borehole *2* as an injection point) and in the boreholes *1* – *5* (when using borehole *3* as an injection point). The electrodes are metal plates bent around the cable, with a size similar to a normal take-out in an ERT cable – thus a cylinder of about 5 cm length and 1.5 cm diameter. The maximum investigation depth reached by the ERT surveys was about 9.2 m from the ground surface, with the first electrode in each borehole positioned just below the water table, that was at about 3.6 m depth at the time of the experiment. The repeated electrical surveys were performed using an IRIS Syscal Pro resistivity meter. For each survey, an acquisition scheme composed of “skip 1” (i.e. made of dipole with length twice the electrode separation – thus, in this case the dipole size is 0.8m) dipoles (AB - MN) and a cross-hole bipoles (AM - BN) was used, with a total number of 652 quadrupoles, including 388 cross-hole bipoles and 264 skip 1 dipoles. A total acquisition time of about 20 minutes was needed for each acquisition. A complete reciprocal scheme acquisition was performed for a correct estimation of measurement errors (see, *e.g.,* Tso et al., 2017). For the inversions, only data satisfying a maximum 10% reciprocal error were used.

The data quality is generally good, but not excellent. On average, over all time steps, only 61% of the quadrupoles satisfy the 10% reciprocal error threshold, with a slight predominance of dipoles (69%) over bipoles (56%). Note also that, in general, dipoles provide higher resolution images and are not fraught with symmetry uncertainties issues (left-right) as bipoles are. A graph showing the evolution of errors is reported in Figure 4, where it is apparent how there is no apparent trend of errors over time.

5 INVERSION OF THE ELECTRICAL DATA SETS

In this paper the inversion of electrical data sets was performed using an Occam inversion approach, which seeks to find the spatially smoothest model that fits the data within a specified *a-priori* value of the measurement errors, as described by deGroot-Hedlin and Constable (1990). The smoothness of the calculated resistivity distribution depends on the error level in the data sets. LaBrecque et al. (1996b) showed that a noise overestimation may result in excessively smooth model, while noise underestimation may lead to artificial image structures. Noise estimation is hence an important factor to be considered before the inversion set up. In the present study the error level assessment was obtained by the analysis of reciprocal error, defined by Binley et al. (1995) as follow:

$$e = \frac{|R_n - R_r|}{(R_n + R_r)/2} \% \qquad (1)$$

where R_n is the 'normal' resistance measurement and R_r is the 'reciprocal' resistance measurement, in which current and potential electrode pairs are reversed. Theoretically R_n and R_r shall be equal, due to the reciprocity theorem (Parasnis, 1988): any deviation from this value may be interpreted as an error estimate. As stated above, in the present study only data satisfying a maximum 10% reciprocal error were used.

The inversion of electrical resistivity data was performed using the code *R2* (Lancaster University, UK), which is a forward/inverse solution for 2D/3D current flow in a quadrilateral or triangular mesh. A quadrilateral mesh was here used, which includes 61 nodes along the horizontal (x) direction and 71 nodes along the vertical (z) direction, for a total number of 4200 quadrilateral finite elements - the region between the boreholes is discretized more finely, honouring the presence of two element sides per vertical electrode separation. The removal of singularity components from the total potential field (Coggon, 1971; Lowry et al., 1989), which are responsible for poor numerical approximations particularly close to the electrode positions, helped improve computational performance.

Changes in ERT images with time as registered during the tracer test were analysed according to the simple ratio approach of Daily et al. (1992). The data to be inverted were derived from the ratio between electrical resistance values measured at the same quadrupole at different acquisition times (R_t) with respect to the background resistance value (R_0) as follow:

$$R = \frac{R_t}{R_0} R_{hom} , \qquad (2)$$

where the term R_{hom} is the resistance for a homogenous resistivity distribution model (chosen to have a uniform resistivity of 100 Ωm). The same approach has been successfully used for similar applications, as demonstrated in the recent literature (*e.g.* Cassiani et al. 2006, 2009). In all cases and L2 norm was adopted for data fitting, within an Occam inversion scheme as described, e.g., in Binley and Kemna (2005). In the ratio inversion approach, a common set of quadrupoles was used that is present in all seven time-step surveys, in order for results to be comparable. In all cases, convergence was assumed once chi-squared measure of data misfit (as defined by Günther et. al., 2006) was unity.

6 RESULTS

In order to avoid redundant interpretations and conclusions, the results that will be shown in the following paragraphs refer only to ERT data measured at the 2D section between boreholes *1* and *5*. The resistivity patterns obtained by the cross-hole ERT investigation along the borehole pair *1 – 4* are very similar and add little to the overall picture.

6.1 Background surveys

To collect the background data set necessary for the comparison with the electrical resistivity data acquired during and after tracer injection, a complete cross-borehole acquisition was performed before the injection of the NaCl brine, along the 2D section between boreholes *1-5*. The main result of the *time 0* survey in terms of resistivity is shown in Figure 5. Note that the electrical resistivity pattern is plotted between 3.6 m to 9.2 m depth: the vadose zone is not shown in this section as no electrode is placed above water level and very scarce information is available in that region. The double-packer chamber that has been used for injection is placed approximately between 7.5 and 8 m depth (shown by the white rectangle in Figures 5, 6, 7)

The electrical resistivity results confirm the stratigraphy as inferred from geological field investigations (Figure 5); in particular, note on the 2D ERT section the presence of:

(1) a first layer between about 3.6 m to 6 m characterized by relatively low resistivity values (around 10 - 20 Ωm) that corresponds to the layer of silty soil as indicated by drilling logs;

(2) a deeper layer characterized by electrical resistivity values that gradually increase with depth to maximum value of 70 Ωm, roughly corresponding to the zone of sand with gravel placed between 6 and 14 m along the stratigraphic sequence.

6.2 Injection and post – injection

The injection of the tracer test was monitored continuously via cross-borehole ERT from the injection time and for about five hours. The results of the experiment shown as images of resistivity can be seen in Figure 6. Strong changes are clearly present over time as a consequence of brine migration. During the injection of the saline tracer (*time 1* – at about 00:10 hours after the start of injection), a decrease in resistivity with respect to *time 0* values is noticeable in the central part of the 2D section, immediately above the injection chamber, at a depth range between 6 and 7 m from the ground surface. However, some small increase in resistivity is apparent around this low resistivity body, both below and on the sides. These artefacts become stronger, together with the low resistivity signature at the centre of the image, immediately after the end of injection (*time 2* – at 00:30 hours after the start of injection) and reach a maximum at *time 3* and *time 4* (at 01:00 and 03:00 hours after the start of injection, respectively). Subsequently, due to the introduction of non saline water in the injection system, the system returns to pre-injection conditions at the end of the experiment (see *time 5* and *time 6, i.e.* at approximately 04:00 and 04:30 hours after the start of injection).

The most striking feature of these results is obviously the apparent increase in resistivity, which practically invades the entire cross-section below the water table and has maxima flanking the boreholes on both sides. This pattern is clearer in the ratio inversion results (Figure 7) obtained using the ratio inversion approach described above and the *time 0* as reference time. The values in Figure 7 are shown in terms of ratios (in %) with respect to the *time 0* resistivity distributions: 100% means no change with respect to background, values less than 100% indicate a decrease in resistivity (which are attributed to increases in pore fluid conductivity caused by the saline tracer). The anomalous high peak in resistivity is well distinguishable at time-lapse images *3 over 0* and *4 over 0*. The most likely explanation of this high resistivity phenomenon is the rapid arrival of the brine to the boreholes via the opened fractures, thus not necessarily invading the entire surrounding medium. The boreholes, once invaded by the brine, act as high-conductivity short circuits, reducing dramatically the current flux into the surrounding porous medium, which thus appears to be more resistive than before brine injection. This is equivalent to reducing the current patterns to quasi-1D along the boreholes rather than 3D as under normal conditions. The above artefacts, peculiar to the borehole effect described in the previous sections, mask nearly completely the migration of the brine in the porous medium itself and make interpretation difficult from a hydrogeological point of view.

The rapid boreholes filling with saline solution is confirmed by the down-hole electrical conductivity measurements in boreholes *1*, *5* and *6*, as shown in Figure 8. The conductivity meters immediately after the end of injection recorded high values of conductivity compared to the background (*time 0*) conditions. The conductivity value recorded in borehole 5 after the brine injection exceeds the end of scale of the instrument (in this case equal to 20 mS/cm). The short time required for the brine to reach the neighbouring boreholes is a certain indication of the occurrence of hydraulic fracturing. Note, in particular, the increase of conductivity values in boreholes *1 – 5*, which have been used for cross-hole ERT.

7 SYNTHETIC MODELLING

In order to obtain an indirect confirmation that the rapid arrival of the brine to the boreholes cause them to act as short circuits, reducing dramatically the current flux into the surrounding media and causing the borehole effect, we modelled the plume migration and its effect in terms of electrical resistivity variations by performing several 2D and 3D synthetic simulations. The inversions for 2D cross-hole ERT synthetic data were performed, as for the field data, using the code *R2*. In order to simulate the evolution of the system resistivity as a consequence of the saline plume migration, a 3D resistivity forward modelling was performed using the code *R3t* (Lancaster University, UK). For the 2D inversions we used the same mesh used for field data while the forward 3D mesh is made of triangular prisms (see Zienkiewicz et al., 2005) for a total of 172,032 finite elements; a finer discretization has been used close to the two measurement boreholes *1* and *5*, with node spacing of the order of 0.01 m in the horizontal direction. This resolution level allows to model accurately the borehole geometry and the fluids therein, being the borehole diameter equal to 2 inches (0.0508 m). The 3D triangular prism mesh was formed by extruding vertically a triangular mesh in the horizontal plane.

As for the field case, a measurement scheme composed of a skip 1 dipole (AB-MN) and a cross-hole bipole (AM-BN) configurations was used, using a total of 259 electrodes combinations. Note that while each cable had 24 electrodes, only 30 of the 48 electrodes were actually utilized, as the water level was at about 3.6 metres below ground. The

2D/3D forward and inverse solutions that will be here shown have been obtained with the removal of singularity errors, as described for the field results.

7.1 Background model

As a first step of synthetic modelling, we created a background model. We took the electrical resistivity distribution as reconstructed by the borehole ERT background acquisition (Figure 9 – left panel) and created a 3D forward model on the basis of a simple one-dimensional layering (Figure 9 – central panel). This reference model has been constructed to incorporate three layers:

1) a shallow layer between 0 and 3.6 m below ground, which represents the vadose zone;
2) a second layer between 3.6 and 6 m below ground surface, which represents the shallowest part of the saturated zone, corresponding to the saturated silty soil;
3) a third layer between 6 and 12 m below ground, representing the saturated sand/gravel layer.

The 3D forward solution calculated in this way has been subsequently used to solve a 2D inverse problem with the same acquisition scheme as used in the field case, i.e. to reproduce synthetically the *time 0* image. A trial-and-error procedure, which only aimed at identifying the order-of-magnitude values for the layer resistivity, led to accepting the following values as reasonable for the electrical resistivities of the three layers:

- upper layer (unsaturated silt layer): 60 Ωm
- middle layer (saturated silt layer): 20 Ωm
- bottom layer (saturated sand/gravel): 40 Ωm

The result is shown in the right panel of Figure 9. Note the good correspondence between the real dataset and the synthetic one, the latter showing the presence of two layers very similar to the true case and a contrast in electrical resistivity at a depth value of about 6 m from the ground surface. Note however that the real data seem to show a more gradual transition between silt and sand/gravel than hypothesized in the synthetic modelling. On the other hand, our purpose here is not to match the experimental results perfectly (which could be done by adjusting the resistivity distribution) but rather to give a reasonable explanation of the observed ERT results, particularly to act as a "background" image for synthetic time-lapse modelling.

7.2 Plume evolution model

Once a reasonable pattern for the synthetic *time 0* image was obtained, we computed several 3D forward solutions to reproduce a possible, simplified plume migration through such a stratified model. Figure 10 shows the conceptual evolution of the synthetic plume from *stage A* (background) to *stage E*. These different stages are constructed to produce synthetic results that can be compared against the field results in order to derive some understanding of the actual saline tracer movement during the field experiment. The value of electrical resistivity of the synthetic tracer, which is modelled as a 3D cylinder with variable radius and height during the time, has been set to 0.1 Ωm (this value being comparable to that of the true saline solution used in the pilot-field). The five panels in Figure 10 refer to a 2D vertical section (along the x-z directions) of the 3D model used for the forward background calculation. Note in particular *stage E*, when we hypothesized that the conductive brine reaches and invades the boreholes *1* and *5* at a depth range between 3.6 m to 9.2 m. The 3D ERT dataset calculated in this way have been subsequently inverted in accordance with the cross-borehole scheme adopted in the field.

A selection of key results is shown in Figure 11 and in Figure 12. In particular, the images in Figure 11 show the results of the synthetic modelling in terms of resistivity which can be compared to the real tomograms. The synthetic results confirm that it is possible to detect the plume migration in the subsurface (consider *stages A* to *D*) until the saline tracer invades the boreholes (*stage E*). At this final stage the *borehole effect* becomes predominant, masking nearly entirely the true resistivity pattern. Note how this short circuit effect is clearly highlighted by the ratio inversion results of Figure 12. A comparison between the actual field results at different times with the synthetic results shows clearly how stage E is reached in the field as early as *time 2*, i.e.00:30 hours after the start of tracer injection, with some evidence of the developing borehole invasion already at *time 1* (at 00:10 hours after the start of the experiment). In the field the stage E condition is maintained till fresh water reaches the boreholes (*time 5*) and washes out the brine (*time 6*).

8 DISCUSSION AND CONCLUSIONS

We have presented an example of ERT time-lapse monitoring of hydraulic fracturing of low permeability sediments for remediation purposes. As a very saline tracer is generally used to monitor such fracturing via down-hole conductivity meters, in principle ERT is a viable and powerful technique to monitor the development of fractures and to assess the invaded volume. This information is extremely valuable for the design of the in situ remediation procedures. However, we demonstrate how ERT can be severely affected by the rapid uncontrolled invasion of the monitoring boreholes by the fast-moving brine in the developed fractures. A strong borehole effect blinds the ERT capability of imaging the region between the boreholes. In our study even a simplified synthetic model is capable of reproducing, to a fair degree of accuracy, the field results once the boreholes are invaded by the brine, thus confirming our explanation of the observed and apparently paradoxical field evidence.

In principle such a borehole effect could be modelled and removed from the field data, in order to extract only the information coming from the region outside the boreholes. However such an approach would require that two key assumptions are satisfied:

(a) applicability of Ohm's law, that would ensure linearity of the system and superposition of effects;

(b) the existence of a relatively low resistivity contrast between boreholes and surrounding formation, once the boreholes are filled with the brine. This would guarantee that some non-negligible fraction of current travels outside the boreholes themselves.

Unfortunately, neither of the conditions above can be reasonably ensured. Assumption (a) is also a pre-condition for the applicability of the reciprocity theorem (Parasnis, 1988) and in fact the field data have a poor reciprocal error level (we had to use a high 10% threshold level to preserve a sufficient number of surviving resistance data). While there may be a few reasons for this fact (Wenner, 1912), the high salinity of the tracer may be the main reason, violating Ohm's law. Assumption (b) is also difficult to satisfy, as the rapid migration of the brine through the induced fractures is likely to fill the boreholes of conductive brine and leave the surrounding formation largely unaffected and filled with the much more resistive formation water. This mechanism is also indirectly confirmed by the speed of the insurgence and disappearance of the borehole effect, which is only compatible with fast fracture flow through the system.

All the limitations above do not imply that ERT is not a viable monitoring technique, provided that a less saline solution is used for hydraulic fracture monitoring. The use of a dense brine has, in fact, little justification other than to ensure that some signal is clearly visible in the down-hole conductivity meters. Given the imaging capabilities of ERT such a strongly conductive solution is not only unnecessary, but as shown here, detrimental to the ERT information content. A NaCl solution of the order of 6 g/l, as normally used in saline tracer experiments, is largely sufficient also for the monitoring of hydraulic fracturing, and we strongly suggest not to exceed such values.

Our study highlights the value of scenario modelling to improve interpretation of monitored data, and the risk of false interpretation if such a task is not performed.

9 ACKNOWLEDGEMENTS

We acknowledge partial support from the research funds of Fondazione CARIPARO ('Dottorati di ricerca - 2008' Project). We also wish to thank prof. Gianni Andreottola and prof. Alberto Bellin (both at the University of Trento) for directing our attention to this case study and Dr. Emanuele Bena (Gamut s.r.l, Torino) for support with the field acquisition.

10. DATA AVAILABILITY STATEMENT

Data used in this paper will be made accessible on the University of Padova Data Repository (http://bibliotecadigitale.cab.unipd.it/en/publishing_EN/Research%20Data%20Unipd).

11. REFERENCES

Binley, A., Cassiani, G., Middleton, R., Winship, P., 2002. Vadose zone flow model parameterisation using cross-borehole radar and resistivity imaging. Journal of Hydrology, 267(3-4), 147-159.

Binley, A. and A. Kemna, 2005, DC resistivity and induced polarization methods, in: Hydrogeophysics, Springer, 129–156.

Binley, A., Ramirez, A. and Daily, W., 1995. Regularised Image Reconstruction of Noisy Electrical resistance Tomography Data, in: Beck, M.S., Hoyle, B.S., Morris, M.A., Waterfall, R.C., Williams, R.A. (Eds.), Process Tomography — 1995. Proceedings of the 4th Workshop of the European Concerted Action on Process Tomography, Bergen, 6–8 April 1995, pp. 401– 410.

Busato L., J. Boaga, M.T. Perri, B. Majone, A. Bellin, G. Cassiani, 2019, Hydrogeophysical characterization and monitoring of the hyporheic and riparian zones: the Vermigliana Creek case study, Science of the Total Environment, 648 (2019), 1105-1120. doi: 10.1016/j.scitotenv.2018.08.179.

Camporese, M., Salandin, P., Cassiani, G., Deiana, R., 2011., Assessment of local hydraulic properties from electrical resistivity tomography monitoring of a three-dimensional synthetic tracer test experiment, Water Resources Research, 47, W12508, doi:10.1029/2011WR010528.

Camporese M., G. Cassiani, R. Deiana, P. Salandin and A. Binley, 2015, Coupled and uncoupled hydrogeophysical inversions using ensemble Kalman filter assimilation of ERT-monitored tracer test data, Water Resources Research, 51(5), 3277-3291, doi: 10.1002/2014WR016017**.**

Cassiani, G., Godio, A., Stocco, S., Villa, A., Deiana, R., Frattini, P., Rossi, M., 2009. Monitoring the hydrologic behaviour of steep slopes via time-lapse electrical resistivity tomography. Near Surface Geophysics, special issue on Hydrogeophysics, 475-486.

Cassiani, G., Bruno, V., Villa, A., Fusi, N., Binley, A.M., 2006. A saline tracer test monitored via time-lapse surface electrical resistivity tomography. Journal of Applied Geophysics, 59, 244-259.

Coggon, J.H., 1971. Electromagnetic and electrical modeling by the finite element method, Geophysics, 36, 132–155.

Coscia I., N. Linde, S. Greenhalgh, T. Vogt, A. Green, 2012, Estimating traveltimes and groundwater flow patterns using 3D time-lapse crosshole ERT imaging of electrical resistivity fluctuations induced by infiltrating river water, Geophysics, 77(4), E239-E250, doi: 10.1190/GEO2011-0328.1.

Crestani E., M. Camporese, P. Salandin, 2015, Assessment of hydraulic conductivity distributions through assimilation of travel time data from ERT-monitored tracer tests, Advances in Water Resources, 84, 23-36, doi: 10.1016/j.advwatres.2015.07.022.

Daily, W., Ramirez, A., Binley, A., LaBrecque, D., 2005, Electrical resistance tomography—Theory and practice: in Butler, D. K. (Ed), Near surface geophysics, SEG Investigations in Geophysics, Series No. 13, 525–550.

Daily, W.A., Ramirez, A., Binley, A., LaBrecque, D., 2004. Electrical resistivity tomography. Leading Edge, 23(5), 438–42.

Daily, W., Ramirez, A., 1995. Electrical-resistance tomography during in-situ trichloroethylene remediation at the Savanna River site. Journal of Applied Geophysics, 33, 239–249.

Daily, W., Ramirez, A., LaBrecque, D., Nitao, J., 1992. Electrical resistivity tomography of vadose water movement. Water Resources Research 28 (5), 1429– 1442.

Day-Lewis, F.D., Singha, K., Binley, A., 2005. Applying petrophysical models to radar travel time and electrical resistivity tomograms: Resolution-dependent limitations. Journal of Geophysical Research-Solid Earth, 110 (B8), B08206.

DeGroot-Hedlin, C., Constable, S., 1990. Occam’s inversion to generate smooth, two dimensional models from magnetotelluric data. Geophysics, 55, 1613-1624.

Deiana, R., Cassiani, G., Kemna, A., Villa, A., Bruno, V., Bagliani, A., 2007. An experiment of non invasive characterization of the vadose zone via water injection and cross-hole time-lapse geophysical monitoring. Near Surface Geophysics, 5, 183-194.

Doetsch, J. A., Coscia, I, Greenhalgh, S, Linde, N., Green, A., Gunther, T., 2010. The borehole-fluid effect in electrical resistivity imaging. Geophysics 75, F107, DOI:10.1190/1.3467824.

Günther, T., Rücker, C., Spitzer, K., 2006, Three-dimensional modelling and inversion of dc resistivity data incorporating topography - II. Inversion, Geophysical Journal International, 166(2), pp. 506–517. doi: 10.1111/j.1365-246X.2006.03011.x.

Keller, G.V., Frischknecht, F.C., 1966. Electrical Methods in Geophysical Prospecting, International Series of Monographs in Electromagnetic Waves, vol. 10. Pergamon Press Inc, Oxford, 525 p.

Kemna, A., Binley, A., Day-Lewis, F., Englert, A., Tezkan, B., Vanderborght, J., Vereecken, H., Winship, P., 2006. Solute Transport Processes, In: Applied Hydrogeophysics, Vereecken H. et al., (Eds.), Springer-Verlag, Berlin.

Kemna, A., Vanderborght, J., Kulessa, B., Vereecken, H., 2002. Imaging and characterisation of subsurface solute transport using electrical resistivity tomography (ERT) and equivalent transport models. Journal of Hydrology 267, 125–146.

Keys, W.S., MacCary, L.M., 1971. Application of borehole geophysics to water resources investigations, Techniques of Water Resources Investigations of the USGS, Book 2, Ch. E1, Washington, 126 pp.

LaBrecque, D. J., Morelli, G., Daily W., Ramirez, A., Lundegard, P., 1999. Occam's Inversion of 3D ERT data: in: Spies, B. (Ed.), Three-Dimensional Electromagnetics, SEG, Tulsa, 575-590.

LaBrecque, D. J., Ramirez, A. L., Daily, W. D., Binley, A. M., Schima, S. A., 1996a. ERT monitoring on environmental remediation processes. Measurements Science & Technology, 7, 375-383.

LaBrecque, D.J., Miletto, M., Daily, W., Ramirez, A., Owen, E., 1996b. The effects of noise on Occam’s inversion of resistivity tomography data. Geophysics 61, 538–548.

Lekmine G., H. Auradou, M. Pessel, J.L. Rayner, 2017, Quantification of tracer plume transport parameters in 2D saturated porous media by cross-hole ERT imaging, Journal of Applied Geophysics, 139, 291-305, doi: 10.1016/j.jappgeo.2017.02.024.

Lowry, T., Allen, M.B., Shive, P.N., 1989. Singularity removal: a refinement of resistivity modeling techniques, Geophysics, 54(6), 766–774.

Nimmer, R. E., Osiensky, J. L., Binley, A. M., Williams, B. C., 2008. Three-dimensional effects causing artefacts in two-dimensional, cross-borehole, electrical imaging: Journal of Hydrology, 359, 59–70.

Osiensky, J. L., Nimmer, R., Binley, A. M., 2004. Borehole cylindrical noise during hole-surface and hole-hole resistivity measurements: Journal of Hydrology, 289, 78–94.

Parasnis, D.S., 1988, Reciprocity theorems in geoelectric and geoelectromagnetic work, Geoexploration, 25(3), 177-198, DOI: 10.1016/0016-7142(88)90014-2.

Perri M.T., G. Cassiani, I. Gervasio, R. Deiana, A.M. Binley, 2012, A saline tracer test monitored via both surface and cross-borehole electrical resistivity tomography: comparison of time-lapse results, Journal of Applied Geophysics, 79, 6-16, doi: 10.1016/j.jappgeo.2011.12.011.

Slater, L., Binley, A., Daily, W., Johnson, R., 2000. Cross-hole electrical imaging of a controlled saline tracer injection. Journal of Applied Geophysics, 44, 85-102.

Telford, W.M., Geldart, L.P., Sheriff, R.E., 1990. Applied Geophysics, Second Edition. Cambridge University Press. 645-700.

Tso, C-h, Kuras, O., Wilkinson, P.B., Uhlemann, S., Chamber, J.E., Meldrum, P.I., Graham, J., Sherlock, E.F., Binley, A., 2017, Improved characterisation and modelling of measurement errors in electrical resistivity tomography (ERT) surveys, Journal of Applied Geophysics, 146, 103-119, DOI: 10.1016/j.jappgeo.2017.09.009.

Wenner F., 1912, The four-terminal conductor and the Thomson bridge: U.S. Bur. Standards Bull., v.8, pp 559-610. Resistivity theory.

Zienkiewicz, O.C., Taylor, R.L., Zhu, J.Z., 2005, The finite element method: its basis and fundamentals, Elsevier, 769pp.

Figure 1: Geographical location of the "Trento - Nord" field site in the Trentino – Alto Adige region, North-Eastern Italy (image from www.google.com/earth).

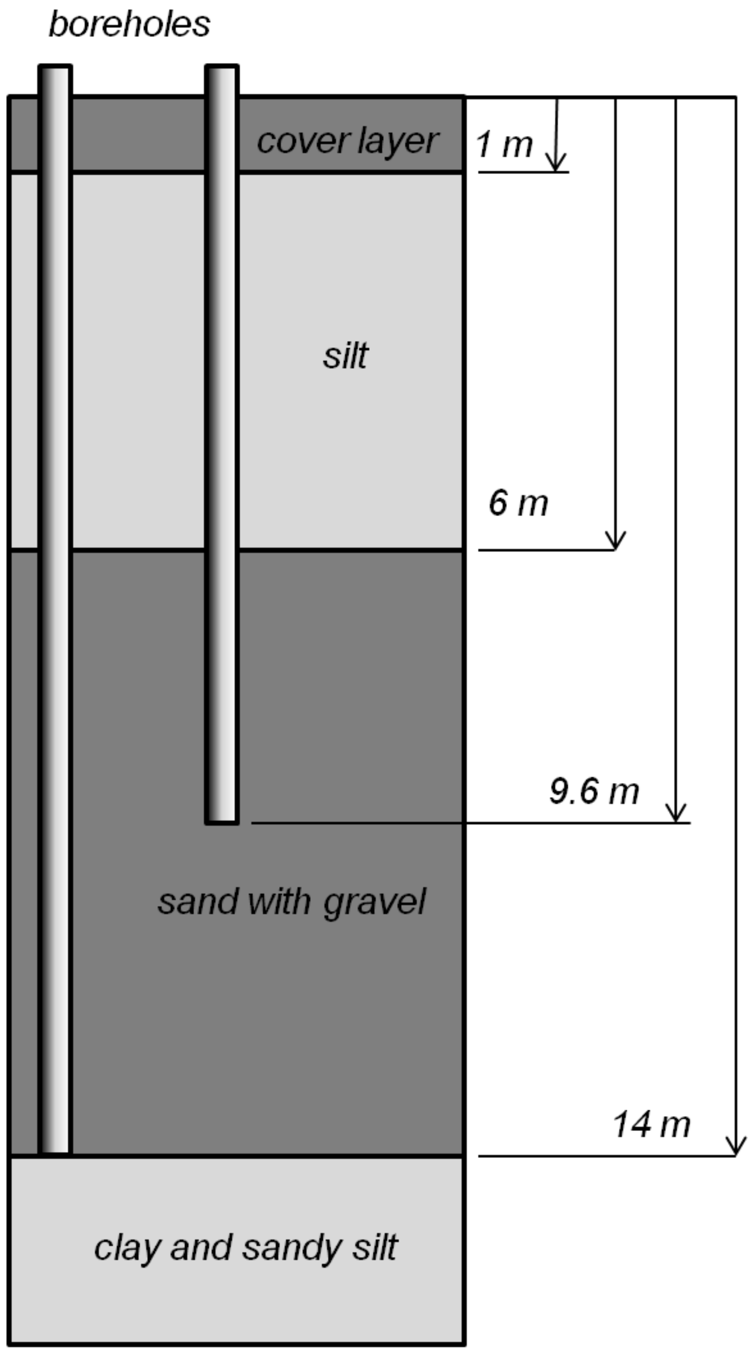

Figure 2: Schematic soil profile of the “Trento – Nord” site from the ground surface to the maximum depth of interest (about 14 m). The stratigraphy can be summarized as a sequence of: a thin layer of man-made debris (about 1 m thick), a layer of silty soil (between about 1 and 6 m), a layer of sand with gravel (between about 6 and 14 m), and a layer of clay and sandy silt with organic matter (from 14 m down).

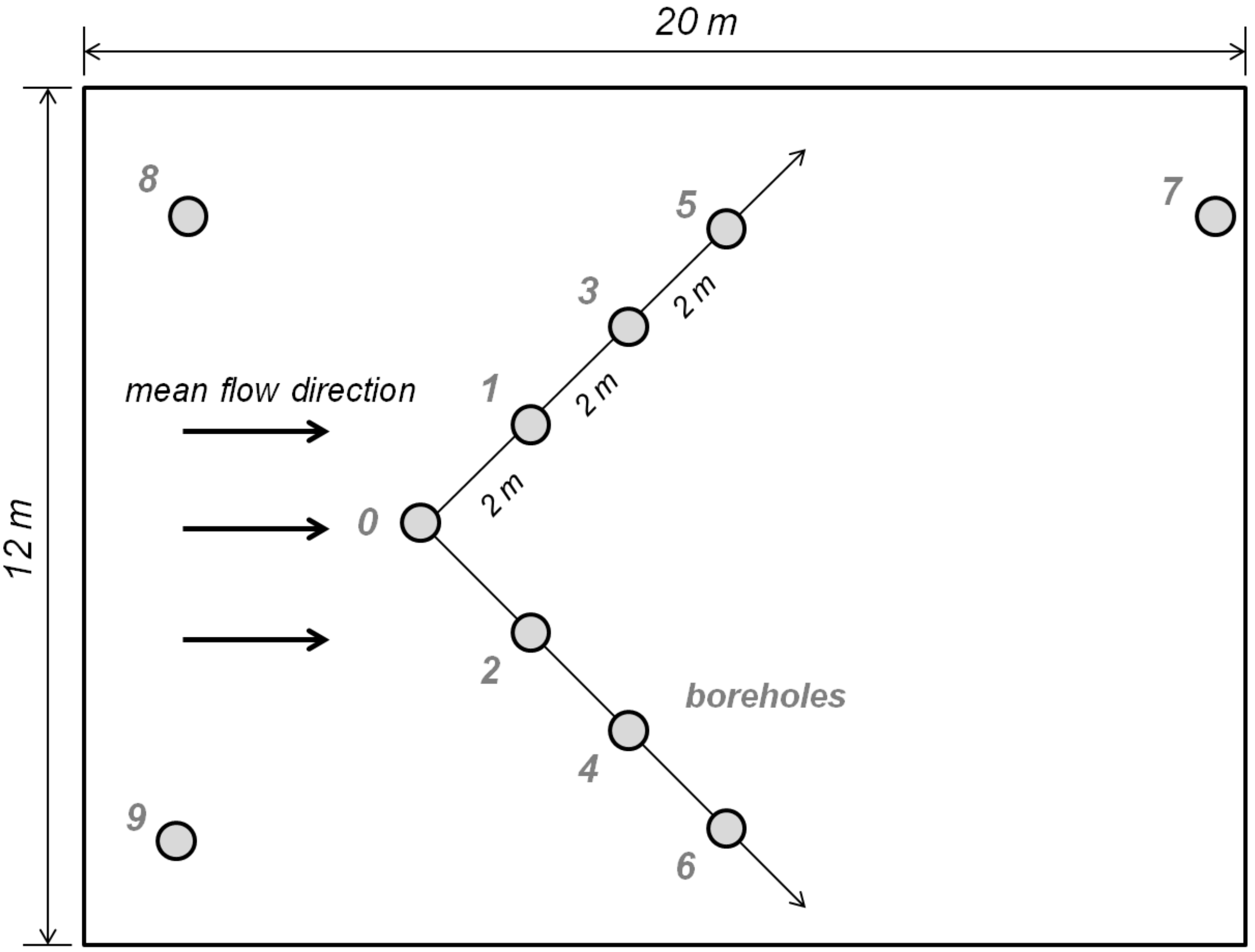

Figure 3: Layout of pilot study borehole array in the "Trento – Nord" experimental site. The boreholes labelled *2* and *3* were used for the injection of the saline solution at two different times, by alternating the pairs *1 – 4* and *1 – 5* as measurement boreholes to collect the time lapse ERT data. For the entire duration of the tracer tests, the electrical conductivity in the aquifer was monitored by the down-hole conductivity meters in all boreholes.

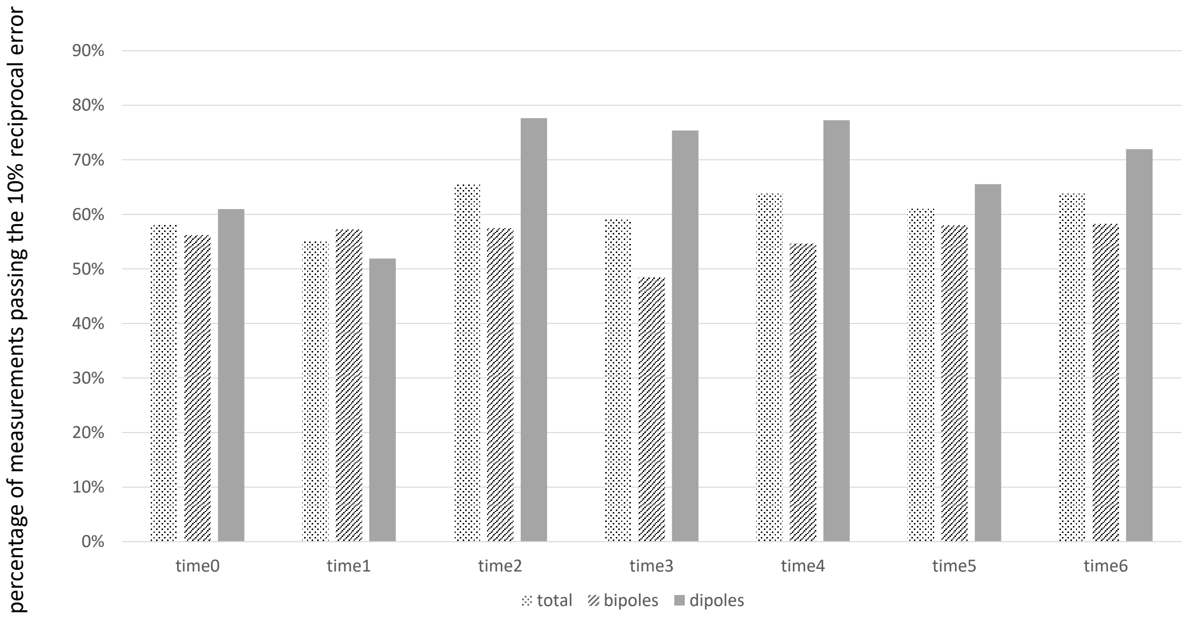

Figure 4: Evolution of quadrupoles surving a 10% reciprocal error check for the seven time-lapse acquisition surveys. On average 61% of data are kept, with a prevalence of skip-1 dipole-dipoles over cross-hole bipoles.

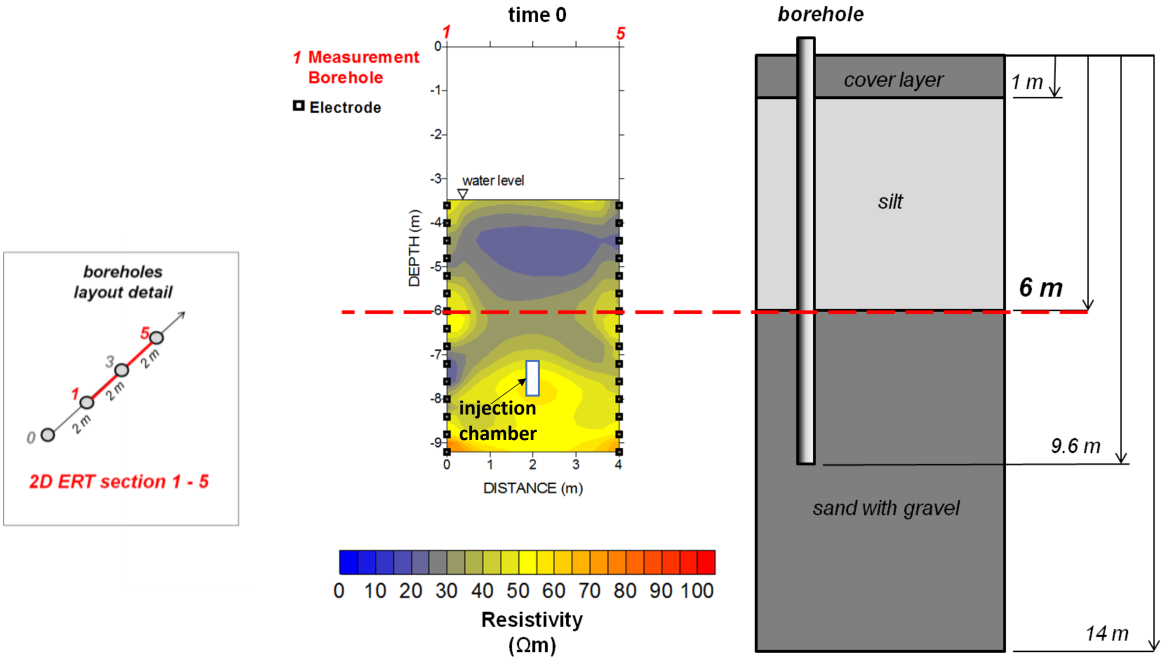

Figure 5: Background resistivity image resulting from the inversion of the cross-borehole ERT data collected at *time 0*, *i.e.* prior to tracer injection, from the borehole pair *1 – 5* (for a plan view of the 2D ERT section see the boreholes layout detail on the left side). The black squares show the electrode locations, with 0.4 m spacing, along each borehole. The results are plotted from -3.6 m down, *i.e.* only considering the saturated zone (the electrodes are all placed below the water table). Note the location of the double-packer injection chamber placed approximately between 7.5 and 8 m in borehole *3* (indicated by a dashed line). The horizontal dashed line indicates approximately the limit between the silty formation (0 to 6 m in depth) and the sand with gravel zone (6 to 14 m in depth).

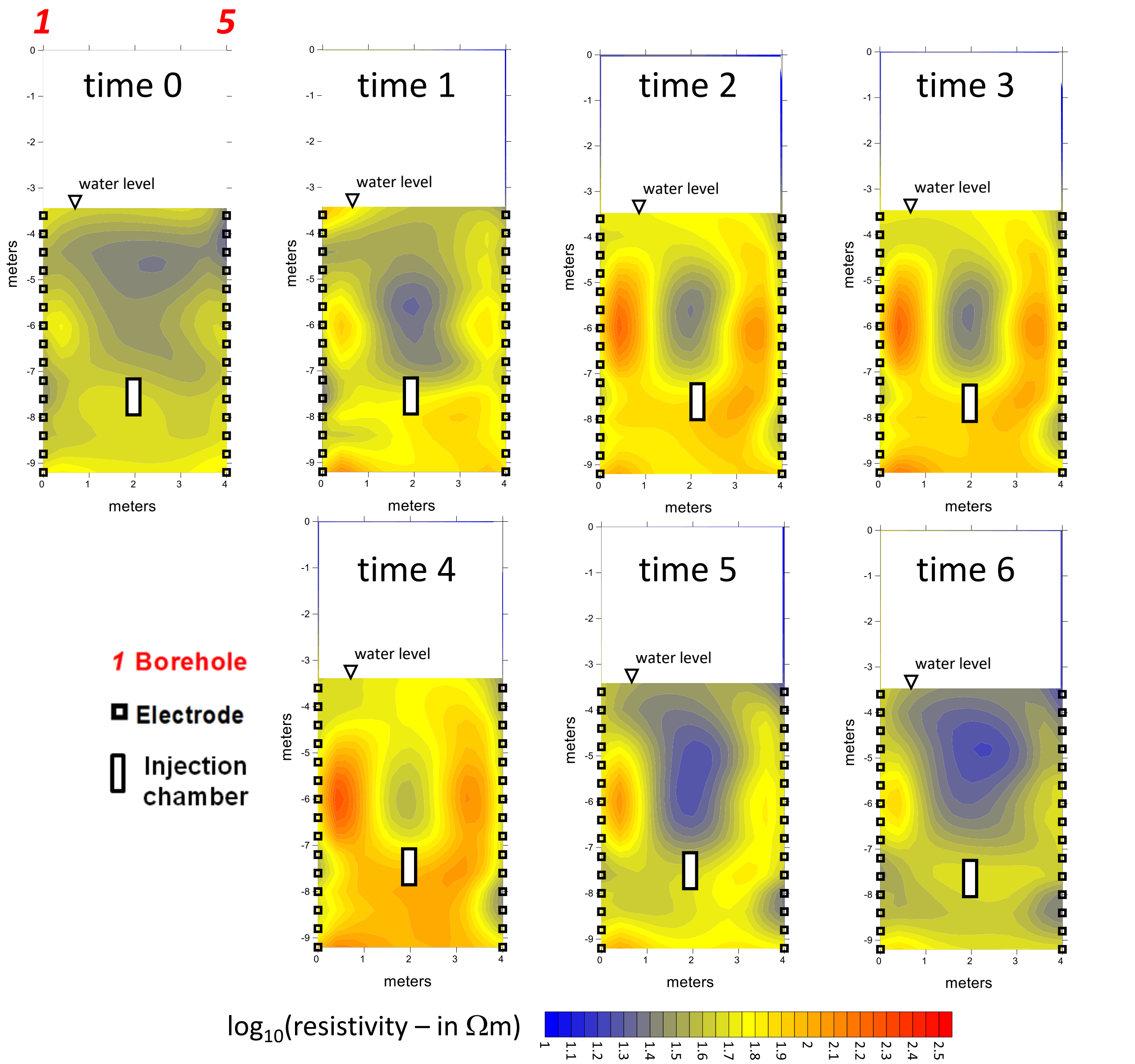

Figure 6: Time-lapse resistivity images during the brine injection experiment. Note the double-packer injection chamber placed approximately between 7.5 and 8 m.

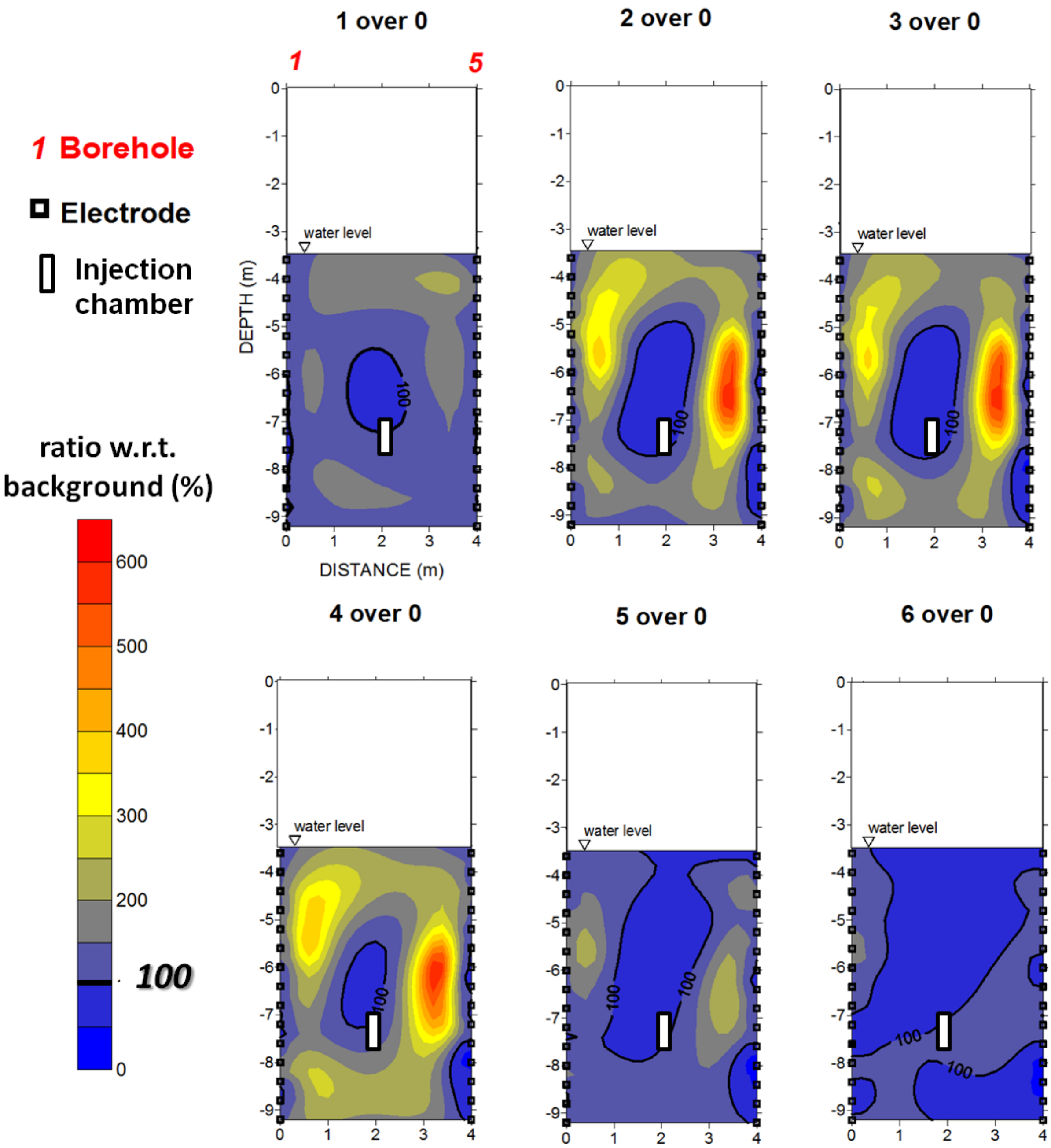

Figure 7: Time-lapse resistivity changes, obtained using a resistivity ratio inversion scheme, during the brine injection experiment. The 100% contour line has been highlighted. Note the double-packer injection chamber placed approximately between 7.5 and 8 m.

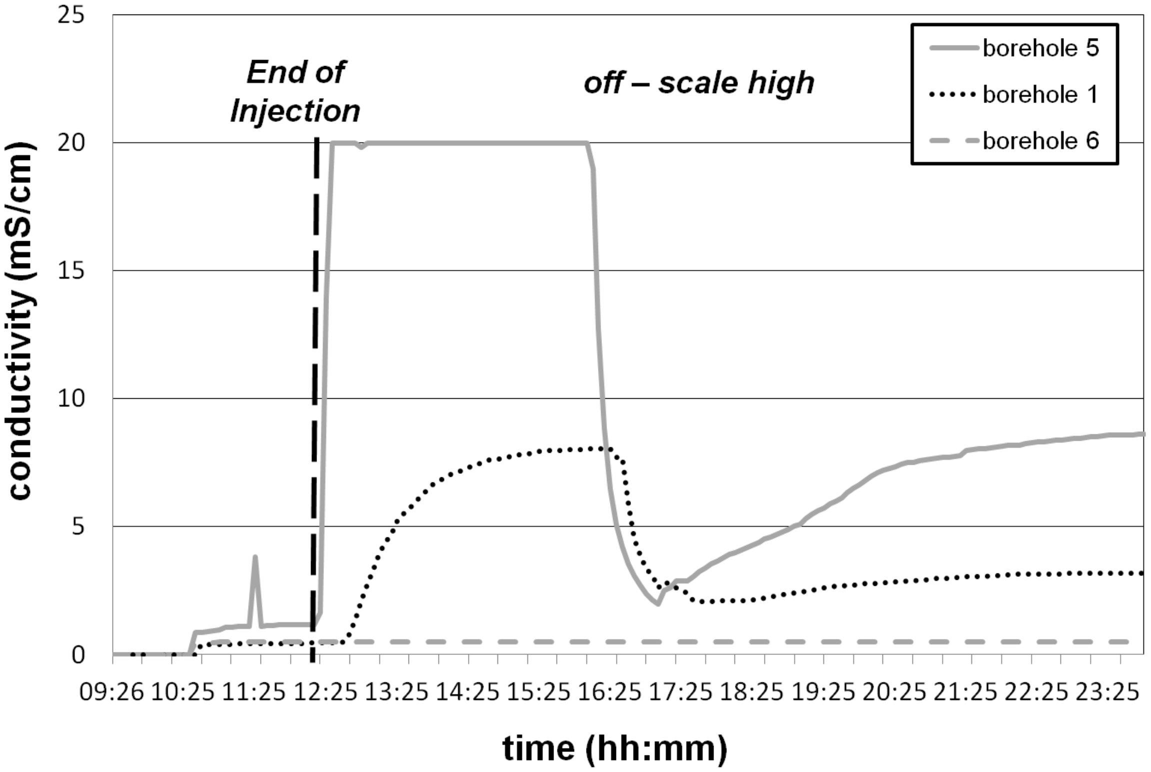

Figure 8: Change in electrical conductivity during the time of field experiment (in hh:mm, local time) as recorded by down-hole conductivity meters. The conductivity meters were placed in boreholes *1*, *5* and *6*, while the injection took place in borehole *3.* Note the rapid increase of conductivity just after the end of injection, at about 12:25, in particular in borehole *5,* where the values went off-scale as shown by the relative curve.

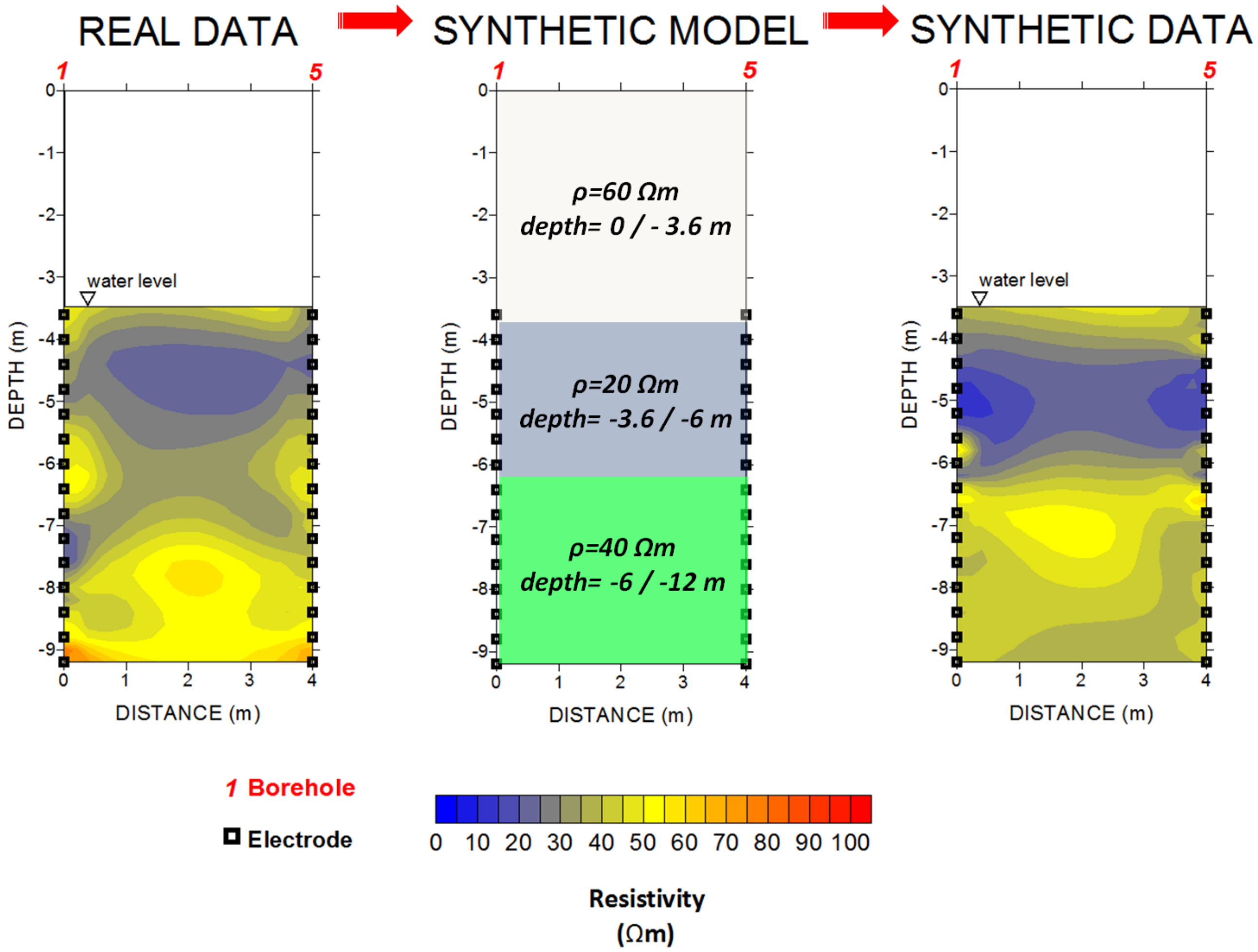

Figure 9: Conceptual scheme illustrating the synthetic reconstruction of a background resistivity distribution (right panel) similar to the field case (left panel). The "true" electrical resistivity model is shown in the central panel.

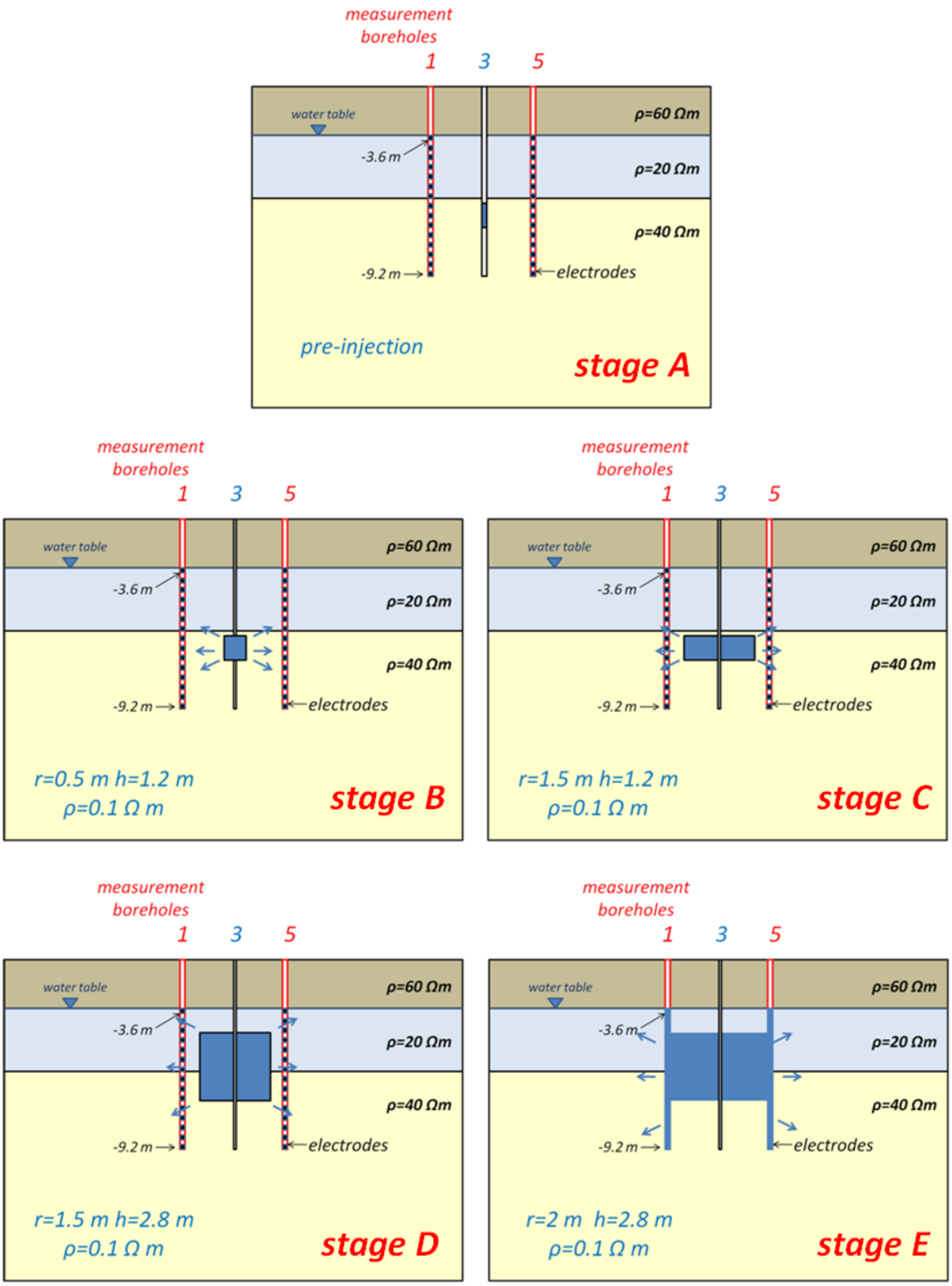

Figure 10: Conceptual sequence illustrating the synthetic plume evolution from *stage A* (background) to *stage E*, when the conductive brine reaches and invades the boreholes in a depth range between 3.6 m to 9.2 m. The sections refer to the x-z plane of a 3D model used for the calculation of the forward solution. The synthetic tracer is represented by a cylinder with an electrical resistivity value of 0.1 Ω m, this value being comparable to that of the tracer used in the field.

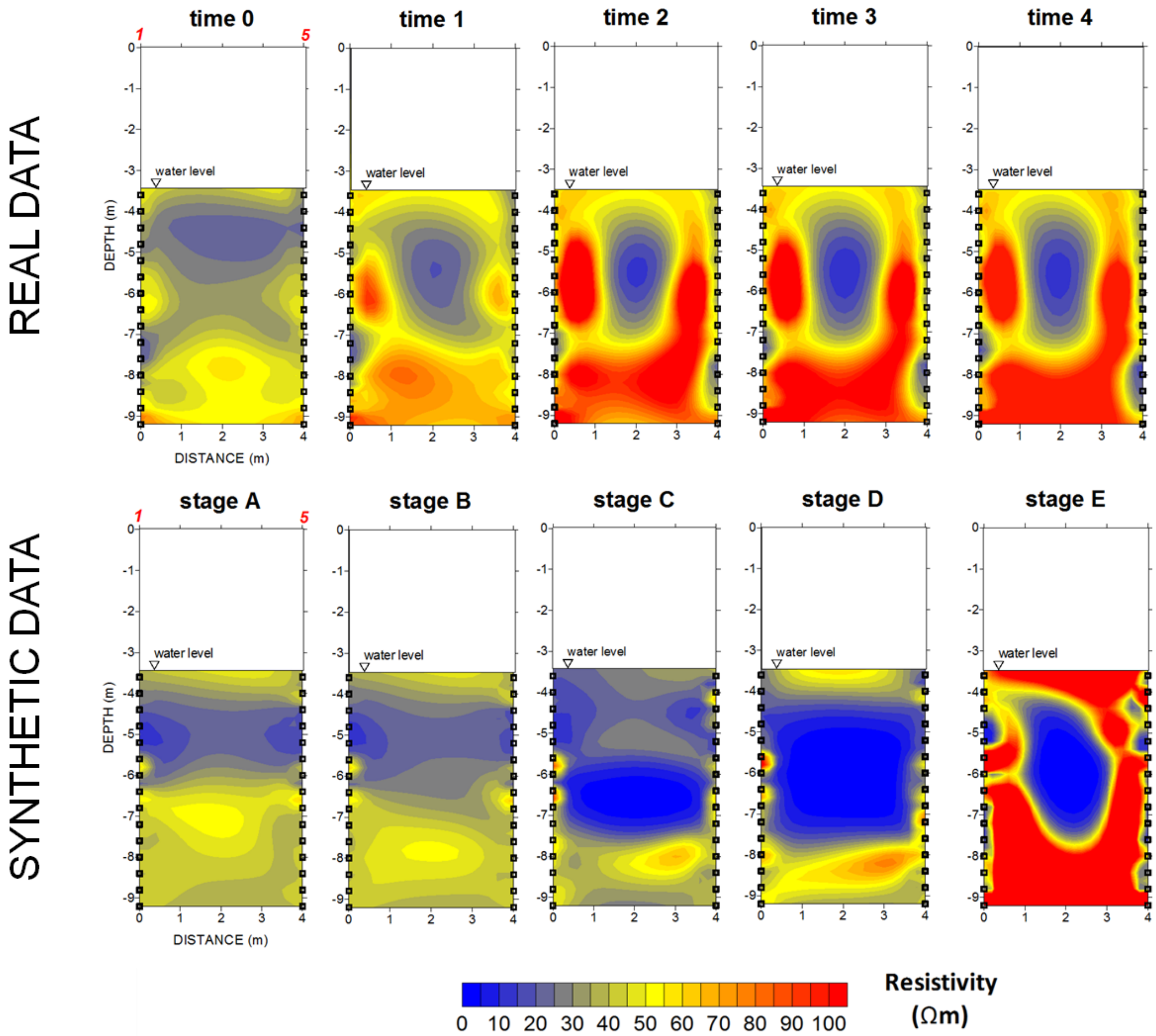

Figure 11: Comparison between real ERT results and synthetic ERT images in terms of electrical resistivity. The synthetic results refer to the variation in resistivity values due to the migration of an imaginary brine solution in the three-layer subsurface model, as shown in Figure 10. Note the good correspondence between real dataset and synthetic one, in particular between the real times *2*, *3* and *4* with the synthetic *stage E*, when we hypothesized that the brine invades the boreholes.

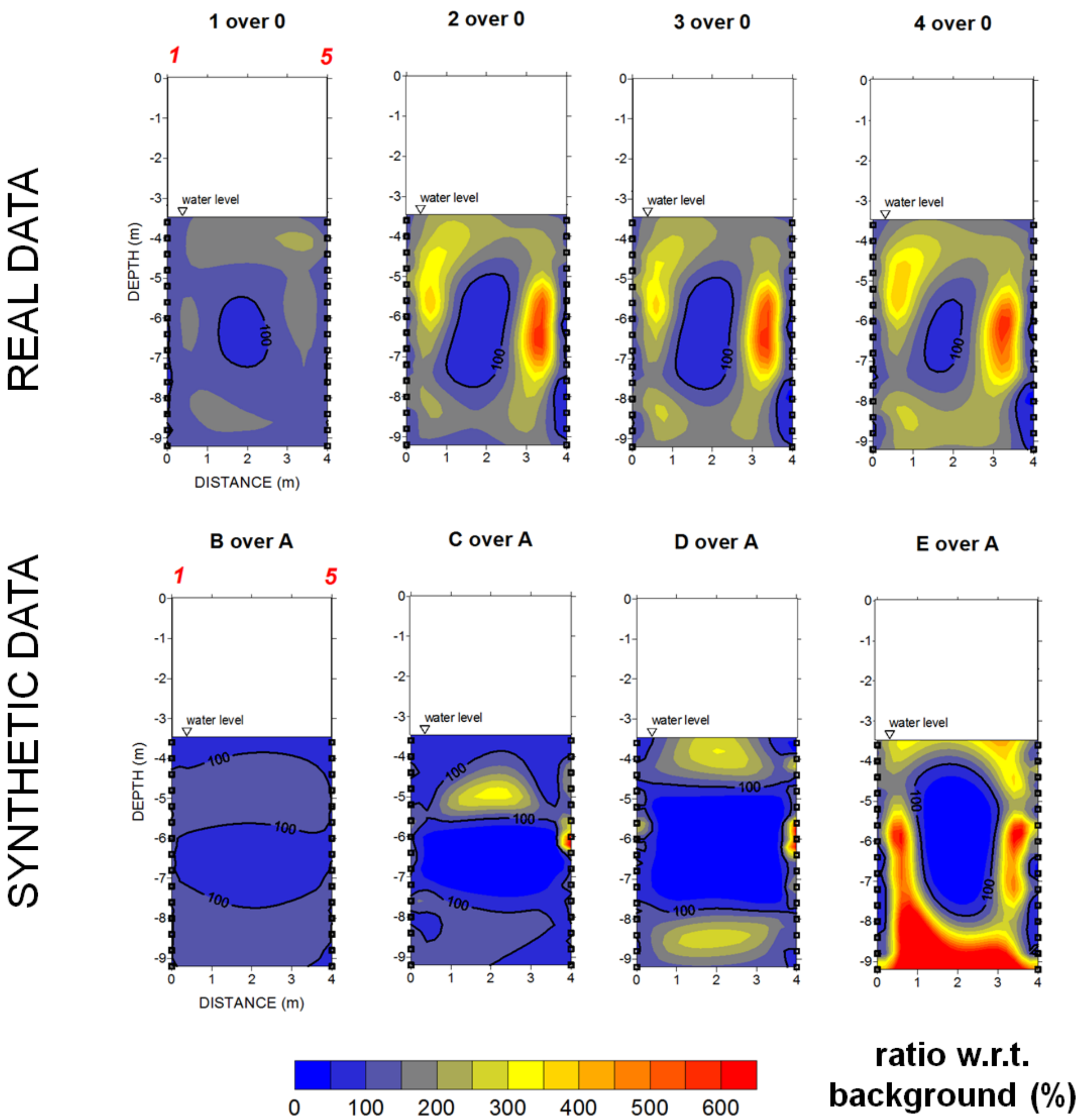

Figure 12: Comparison between real ERT results and synthetic ERT images in terms of ratio of resistivity with respect to the background values (given as %). Note the good correspondence between real dataset and synthetic one, in particular between the real times *2 over 0*, *3 over 0*, and *4 over 0* with the synthetic *stage E over A*, when we hypothesized that the brine reaches the boreholes and causes a borehole effect.